minerals

MDPI

Article

Diagenetic Evolution Mechanism of the Jurassic Tuffaceous Sandstone Reservoir in Qikou Sag, Bohai Bay Basin, East China

Xiuzhang Song [1,2,*], Zhengxiang Lv [1,3,*], Chunyan Zang [2], Peng Hao [2], Yinjun He [2], Wei Zhao [2], Yuanhua Qing [4] and Jie Ren [1,5]

1 College of Energy Resources, Chengdu University of Technology, Chengdu 610059, China
2 CNOOC Experimental Center, Engineering Technology Branch, CNOOC Energy Development Co., Ltd., Tianjin 300450, China
3 State Key Laboratory of Oil and Gas Reservoir Geology and Exploitation, Chengdu University of Technology, Chengdu 610059, China
4 School of History and Geography, Chengdu Normal University, Chengdu 611130, China
5 Sinopec Matrix Xinan MWD/LWD & Logging Corporation, Chengdu 610100, China
* Correspondence: ex_songxzh@cnooc.com.cn (X.S.); lvzhengxiang13@cdut.edu.cn (Z.L.)

Abstract: Exploring for hydrocarbons in a pyroclastic-affected reservoir is an important research topic. Previous studies have mainly focused on laminated pyroclastic. A large number of dispersed pyroclastic is present in sedimentary rocks, and dispersed volcanic ash strongly influences the diagenetic evolution of sandstone reservoirs. However, these aspects remain understudied. We studied the mechanism of the diagenetic evolution of the Jurassic tuffaceous sandstone reservoir in Qikou Sag of the Bohai Bay Basin by performing inclusion temperature measurements, rock slice identification, and scanning electron microscopy, and using electron microprobes and microzone isotopes. We determined the mechanism of water-rock interaction. Based on microscopic observations, we determined that the main diagenesis included two-stage dolomite cementation, two-stage calcite cementation, quartz cementation, and transformation and dissolution of clay minerals. The hydrolysis and chemical transformation of pyroclastic during burial not only provided an alkaline environment in the early stage of diagenesis but also supplied ions for the formation of microcrystalline quartz and early dolomite and the transformation of clay minerals. Leaching and denudation generated early dissolution caused by a tectonic uplift. Following the epigenetic stage, microbial activity stimulated the formation of early calcite during the shallow burial stage. When the burial temperature of the stratum was 80 °C, the acidic fluid discharged from the thermal evolution of organic matter was neutralized by the soluble components in the pyroclastic, which prevented the formation of a large-scale acidic environment. When the burial temperature exceeded 100 °C, the acidic fluid generated by thermal catalytic decarboxylation of organic matter formed a large quantity of dissolution. The dissolution of plagioclase promoted the overgrowth of quartz and the growth of kaolinite.

Keywords: Bohai Bay Basin; Qikou Sag; Jurassic; tuffaceous sandstone reservoir; diagenetic mechanism

check for updates

Citation: Song, X.; Lv, Z.; Zang, C.; Hao, P.; He, Y.; Zhao, W.; Qing, Y.; Ren, J. Diagenetic Evolution Mechanism of the Jurassic Tuffaceous Sandstone Reservoir in Qikou Sag, Bohai Bay Basin, East China. *Minerals* **2023**, *13*, 80. https://doi.org/10.3390/min13010080

Academic Editor: János Haas

Received: 10 November 2022
Revised: 8 December 2022
Accepted: 30 December 2022
Published: 4 January 2023

Copyright: © 2023 by the authors. Licensee MDPI, Basel, Switzerland. This article is an open access article distributed under the terms and conditions of the Creative Commons Attribution (CC BY) license (https://creativecommons.org/licenses/by/4.0/).

1. Introduction

The focus and challenge of reservoir exploration involves studying the mechanisms behind the formation of clastic reservoirs [1–4]. Identifying the evolution of diagenesis in different geological contexts is important for predicting a reservoir. Many geologists have provided valuable information on the diagenetic evolution of clastic reservoirs, such as deep sandstone reservoirs [5–7], medium-shallow depth reservoirs [8,9], eolian sandstone reservoirs [10], deep-water turbidite sandstone reservoirs [11], deep shale gas reservoirs [12,13], etc. While investigating various types of reservoirs, reservoir quality analysis is mainly performed to discuss the mechanism of diagenesis, and many diagenesis models have been constructed to explain the development of reservoirs [14,15]. For example, the coating of particles (such as chlorite and microcrystalline quartz) can inhibit quartz overgrowth or

compaction and help in maintaining the high-quality porosity of deep reservoirs [16,17]. Feldspar dissolution can generate many pores and provide sufficient ions for the creation and transformation of clay minerals and carbonate. This process facilitates the development of a reservoir space [18,19].

Pyroclastic-rich sandstone reservoirs have helped researchers understand clastic reservoirs. Pyroclastic-rich sandstone covers a large portion of the stratum. Huang studied the volcanic ash layer off the coast of New Zealand and found that 64% of the volcanic ash was distributed in the sediment [20]. Scudder et al. showed that the volcanic ash in sedimentary rocks accounts for about 7–30 wt% in the Nankai Trough on the subducting Philippine Sea plate [21]. Some studies were conducted on the hydrocarbon exploration of sedimentary rock reservoirs rich in volcanic ash. Globally, research on pyroclastic-rich sandstones is concentrated in several regions, including China and Japan. White et al. showed that only about 1 wt% of silica cementation developed in the Nankai Trough subduction zone throughout the Shikoku Basin promoted the development of anomalously high porosity. The source of silica was dispersed volcanic ash in sedimentary rocks [22]; however, the transformation mechanism of minerals such as smectite altered by volcanic ash was not discussed by the authors [21]. Khalaf showed that volcanic ash dispersed in the Neoproterozoic terrestrial sedimentary rocks of the Wadi Queih Basin formed chlorite coatings that contributed to the preservation of pores [23]. Lenhardt et al. and Tari et al. showed that studies on the reservoir of volcanic and associated sedimentary rocks were mainly conducted in China [24,25], and a literature review by the authors showed that studies on the effect of dispersed pyroclastic on sandstone reservoirs were mainly conducted in China. The findings of studies from China showed that the influence of dispersed pyroclastic on sandstone reservoirs was reflected in the following two aspects: the coupling of pyroclastic and acid fluid controls the formation of secondary pores, and the devitrification of volcanic glass strongly affects reservoir formation [26–29]. However, the information on the mechanism of the diagenesis of sandstone reservoirs rich in dispersed pyroclastic is limited.

A deep understanding of the mechanism of diagenesis is the key to understanding the petroleum system [30]. For example, the development of carbonate cement can prevent the entry of hydrocarbons. Therefore, the best reservoirs are usually found in areas with low levels of carbonate cement [8,9]. If the diagenetic environment becomes acidic, it can lead to the dissolution of carbonate and other soluble minerals and make the development area of early carbonate cement a favorable site for finding hydrocarbons [11]. However, information on the diagenetic evolution of sandstone reservoirs affected by dispersed pyroclastic is rare. Using the geochemical characteristics of diagenetic materials as constraints can effectively explain the sequence of diagenetic events and apply them to geological exploration, which might help advance research on reservoirs and overcome a long-time challenge for geologists [31–33].

This study mainly focused on (1) determining the diagenetic mineral assemblages associated with the diagenesis of sandstone reservoirs influenced by pyroclastic; (2) using the geochemical information of minerals to study the diagenetic mechanism of dissolution and authigenic mineral cementation under the influence of pyroclastic; and (3) summarizing the mechanism of diagenetic evolution of a sandstone reservoir affected by pyroclastic.

2. Geological Background

The Bohai Bay Basin, located in Eastern China, is a rift lacustrine basin found in North China. The whole basin can be divided into seven depressions [34,35]. Qikou Sag is a secondary rift-subsidence structural unit of the Huanghua Depression in the Bohai Bay Basin and is situated in the central northern part of the Huanghua Depression (Figure 1A). The study was conducted in a part of the slope-faulted structural belt that marks the transition from the slope zone of the southern margin of Qikou Sag to the deep depression zone (Figure 1B), which covers an area of about 1200 km^2.

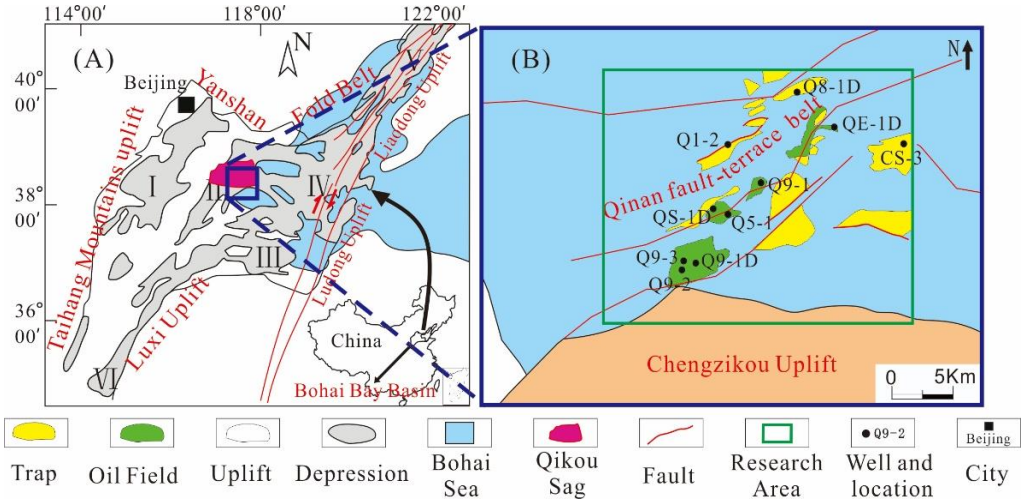


Figure 1. (**A**) A map showing the location of the Qikou Sag and the subunits of the Bohai Bay Basin. The depressions in the Bohai Bay Basin include the Jizhong depression (I), Huanghua depression (II), Jiyang depression (III), Bozhong depression (IV), and Liaohe depression (V) [34,35]. (**B**) A map showing the main well location distribution of Qikou Sag.

Following the Paleozoic area, the burial of the Huanghua depression evolved mainly through three burial-uplift cycles in the Hercynian-Indosinian period, the Yanshanian period, and the Himalayan period [36]. In the Jurassic era, the Huanghua depression entered the rift basin development stage. It was controlled by Pacific Ocean tectonics, characterized by strong volcanic activities, and formed the stratigraphic characteristics of the Jurassic era in Qikou Sag, which is dominated by thick dark mudstone and sandstone, rich in pyroclastic. After the deposition in the Jurassic era, the weak north-south compression structure produced in the late Yanshan Period (Late Cretaceous) uplifted and exposed the stratum until the early Paleogene era, when structural inversion occurred. This event gave rise to the present Qikou Sag strata, which is more than 5000 m thick [37–39].

From the bottom to the top, the strata in Qikou Sag include the Triassic, Middle-Lower Jurassic, Shahejie and Dongying Formations of the Paleoproterozoic, Minghuazhen and Gantao Formations of the Neoproterozoic, and Plain Formation of the Quaternary (Figure 2). We focused on the Jurassic sandstone reservoir in the study area. The Jurassic deposition was discordant and directly beneath the Paleogene (Figure 2); only the Middle-Lower Jurassic remained, which was identified as the Haifanggou Formation in previous studies. It can be further divided into four sections: top, upper, middle, and lower sections. Hydrocarbons are concentrated in the middle and upper sections [40].

Several studies have investigated the characteristics of the reservoir of the Haifanggou Formation in the study area, mainly focusing on four aspects: sedimentary system, lithological characteristics, reservoir space type [41–43], and the main control factors of the reservoirs. However, the process and mechanism of the diagenesis of the clastic reservoir remain understudied. A detailed analysis of the diagenetic events and evolutionary patterns of the reservoirs in the Qikou Sag might provide a reference for reservoir prediction and further characterization of the hydrocarbons of Mesozoic clastic rocks in the Bohai Bay Basin.

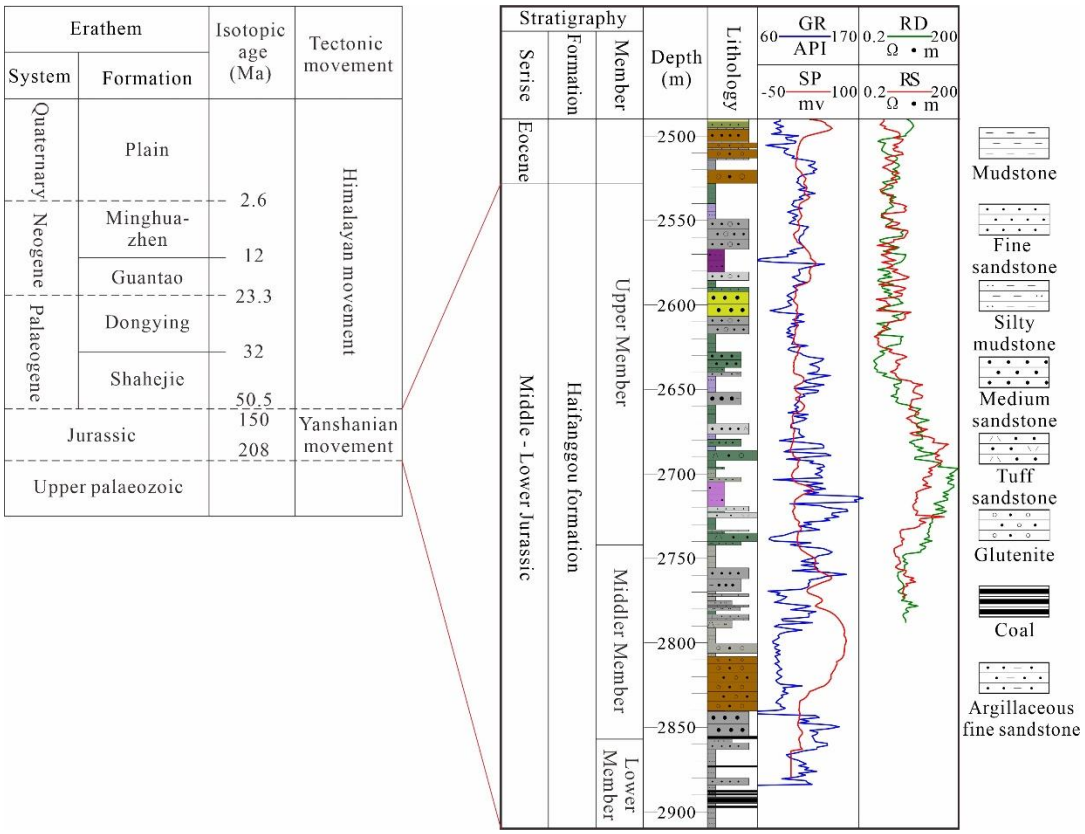


Figure 2. Formation distribution and logging data and lithologic distribution characteristics of a typical well in Qikou Sag (Well Q9-1).

3. Method

The cores were observed and sampled in seven typical wells, and 210 samples were selected to make rock slices. A blue reagent was used to fill the slices, and half of the slices were stained with Alizarin Red. A polarizing microscope was used to observe the microscopic petrological characteristics and perform a preliminary analysis of the authigenic mineral characteristics and occurrence relationships of various diagenesis. Scanning electron microscopy (SEM) was performed to further study the diagenetic characteristics and sequences. To further obtain the geochemical information of diagenesis, typical samples were used for experimental tests of the micro-area isotopes, electron probe microanalysis (EPMA), and the homogenization temperature of the inclusions based on the microscopic characteristics of the minerals. Through diagenesis characteristics, diagenesis time, and geochemical information, the diagenetic mechanism, and evolutionary characteristics of the reservoir were elucidated.

By observing the slices and analyzing the microscopic characteristics of the samples, 48 core samples from six wells were selected for SEM examinations (CARL ZEISS EVO MA15/LS 15). We selected 13 samples rich in authigenic carbonate and processed them to make double-sided polished slices (0.05 mm thick) for micro isotope testing. In the experiment, the carbonate was gasified at the target site using a FUSION CO_2 laser system (focused beam spot 50 μm). Then, the samples were transported to a Finnigan MAT 253 mass spectrometer through a gas enrichment device, and carbon and oxygen isotope values (VPDB standard) were obtained with relative standard deviations of 0.2‰ and 0.3‰, respectively. Next, 12 samples were selected for inclusion homogenization temperature testing, and the samples were cut into double-sided polished slices (0.05 mm thick). The testing instrument included a Zeiss Axio Imager M2 m metallographic microscope and a matching Linkam THMS-600 hot-cold platform, with absolute deviation at 2 °C. Four samples were selected for the EPMA, and the samples were cut into slices (without cover; 0.03 mm thick).

Typical minerals were selected under the microscope, and the elements in the minerals were quantitatively analyzed using the EPMA-1720 series electron probe analyzer.

The EPMA was conducted by the State Key Laboratory of Oil and Gas Reservoir Geology and Exploitation, Chengdu University of Technology (Chengdu, China). The identification of the rock slices, SEM examination, isotope analysis, and the tests on the homogeneous temperature of inclusions were conducted by the CNOOC Experimental Center, Engineering and Technology Branch of CNOOC Energy Development Co. (Tianjin, China)

We used the ancient salinity calculation formula (Formula (1)) derived by Keith and Weber [44] to calculate the ancient salinity.

$$Z = 2.048 \times \left(\delta^{13}C + 50\right) + 0.498 \times \left(\delta^{18}O + 50\right) \quad (1)$$

Here, Z is an indicator of salinity; and $\delta^{13}C$ and $\delta^{18}O$ are PDB standards.

We used the oxygen isotope fractionation equations (Equations (2) and (3)) of the calcite-fluid system proposed by Friedman and O'Neil [45] and the dolomite-fluid system proposed by Fisher and Land [46] to calculate the diagenetic temperatures of calcite and dolomite, respectively.

$$1000 \times \ln \alpha_{calcite-fluid} = 2.78 \times 10^6 \times T^{-2} - 2.89 \quad (2)$$

$$1000 \times \ln \alpha_{dolomite-fluid} = 2.78 \times 10^6 \times T^{-2} + 0.11 \quad (3)$$

Here, T represents the cementation temperature of calcite or dolomite; $\alpha_{calcite \text{ or } dolomite-fluid}$ represents the oxygen isotope fractionation coefficient, which was calculated using the formula $\alpha_{calcite \text{ or } dolomite-fluid} = \left(1 + \delta^{18}O_{calcite \text{ or } dolomite}/1000\right) / \left(1 + \delta^{18}O_{fluid}/1000\right)$; and $\delta^{18}O_{fluid}$ represents the oxygen isotope of the diagenetic fluid; $\delta^{18}O$ represents the PDB standard.

4. Results

4.1. Main Diagenesis

The upper section of the sandstone reservoir of the Haifanggou Formation in the study area had an abundance of dispersed pyroclastic deposited with multiple tuff interlayers; however, tuff was absent in the middle reservoir [40]. After burial diagenesis and structural transformation within a specific geological period, the diagenesis of the middle and upper reservoirs became complex.

4.1.1. Mechanical Compaction

Mechanical compaction in some parts of the study area was strong and weak in others. Strong compaction mainly occurred in the upper section with a large number of matrices and poor particle sorting. The mica present appeared to be bent (Figure 3a), and stylolites were absent. The compaction was weak primarily in areas where authigenic minerals, such as calcite, dolomite, and siliceous substances, were present between particles. Most particles showed point and point-line contact (Figure 3b). Mechanical compaction was inhibited by the distribution of authigenic minerals between particles.

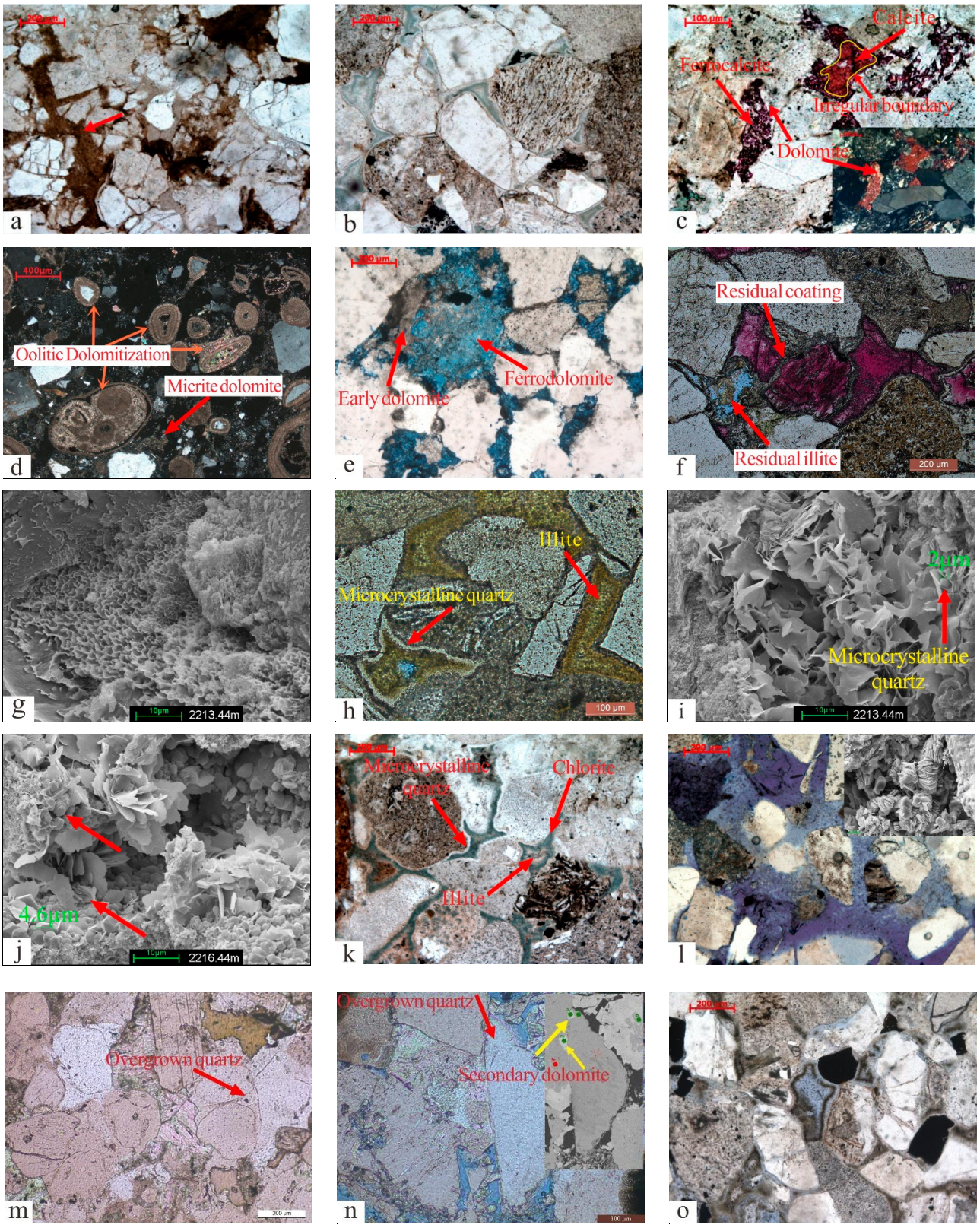


Figure 3. The types of diagenesis. (**a**) Plastic components were compact and deformed (red arrow), QS-1D, 2698.5 m. (**b**) Detrital grains were in point-line contact, and authigenic minerals developed

between particles, Q9-1D, 2672 m. (**c**) Ferrocalcite and calcite filled the dissolution pores, with an irregular boundary between two types of calcite. The dissolution pores contained the residual dolomite due to dissolution, QS-1D, 2427 m. (**d**) Micrite dolomite crystallized between particles, and oolitic was replaced by dolomite, Q9-1D, 2434.45 m. (**e**) Intergranular micrite dolomite was replaced by ferrodolomite, Q9-3, 2409.1 m. (**f**) The coating left by dissolution was covered in ferrocalcite, and the residual illite in intergranular dissolution pores, Q9-3, 2218.01 m. (**g**) Illite/smectite mixed minerals filled the space between particles, Q9-3, 2213.44 m. (**h**) Pores filled with microcrystalline quartz and illite, Q9-3, 2212.58 m. (**i**) Pores filled with flake illite and microcrystalline quartz, Q9-3, 2213.44 m. (**j**) Rose-shaped chlorite formed after microcrystalline quartz (red arrow), Q9-3, 2216.44 m. (**k**) Pores filled with chlorite, microcrystalline quartz, and residual illite, Q9-2, 2033 m. (**l**) Feldspar dissolution left grainy kaolinite, Q9-1D, 2849.7 m. (**m**) Overgrown quartz developed between grains, Q9-3, 2424.26 m. (**n**) Secondary dolomite was encased in overgrown quartz and appeared rhombohedral (yellow arrow), Q9-3, 2423.82 m. (**o**) Intergranular pores formed by the dissolution of clay minerals, Q9-3, 2218.74 m.

4.1.2. Authigenic Minerals

1. Calcite

Authigenic calcite mainly developed in the upper section, and its content ranged from 0.5% to 13% (average 5.01%). It primarily consisted of a continuous crystal structure with a small amount of coarse crystal structure. The calcite in this layer was divided into two phases based on the characteristics of Alizarin Red staining (Figure 3c). The first phase contained ferrocalcite (C1), which mostly filled in the pores formed by the dissolution of feldspar and clay minerals and dyed dark red or purple. Alizarin red-stained late calcite (C2) was found in the pores formed by ferrocalcite dissolution. Irregular erosion boundaries were present between the two-phase calcites (Figure 3c). Calcite (C2) occupied the space formed by the dissolution of ferrocalcite (C1).

2. Dolomite

Authigenic dolomite was found in the upper and middle sections, and its content ranged from 0.5 to 13.5% (average: 4.65%). Based on the occurrence of minerals, dolomite could be subdivided into two phases. Early dolomite (D1) occurred in the form of micrite and powdered crystal, mainly in intergranular pores. Occasionally, a small amount of oolitic dolomitization was found (Figure 3d). D1 was often replaced by late ferrodolomite. Ferrodolomite (D2) consisted of larger crystals and was rhombohedral or had a continuous crystal structure (Figure 3e).

3. Clay Minerals

The study area had various types of authigenic clay minerals. The upper section of Haifanggou Formation comprised illite/smectite mixed minerals, illite, and chlorite, while the middle layer had kaolinite. The percentage of clay minerals varied from 12 to 60%. The average content of clay minerals in the upper and middle sections was 37.5% and 12%, respectively. Illite/smectite mixed minerals adhered to the surfaces of particles as a coating (Figure 3f) or filled in the intergranular pores. The crystal morphology showed honeycomb or flaky patterns (Figure 3g). Illite had similar occurrence characteristics to illite/smectite mixed minerals, showing both coating and filling, and the combination of illite and microcrystalline quartz was common (Figure 3h,i). Chlorite had rose-shaped filled pores (Figure 3j). The symbiotic combination of microcrystalline quartz and chlorite was common. A small amount of illite occasionally remained after being replaced by chlorite (Figure 3k). Kaolinite appeared to be worm-like and was found in the dissolved pores of feldspar (Figure 3l).

4. Quartz

There are two types of authigenic quartz, which include microcrystalline quartz and overgrown quartz.

Most of the microcrystalline quartz was found in the upper reservoir, where illite and chlorite were formed, and it formed a coating around the clastic particles (Figure 3h–k). The length of microcrystalline quartz associated with illite was usually less than 2 μm (Figure 3i), while that associated with chlorite was usually between 2–5 μm (Figure 3j).

Overgrown quartz was found in the middle section where clay minerals did not develop, and it locally filled all intergranular pores (Figure 3m). A part of the overgrown quartz showed inclusions of late dolomite crystals (Figure 3n), indicating the late formation of overgrown quartz.

4.1.3. Dissolution

The complex diagenetic environment of the study area caused the multi-stage dissolution of minerals, such as feldspar, ferrocalcite, and clay. Based on the microscopic characteristics, the dissolution of the minerals could be divided into three stages. Early dissolution caused various minerals to dissolve; most of these minerals comprised feldspar, dolomite, and intergranular matrix. Some residual minerals were preserved after dissolution. Residual clay minerals commonly occurred as coatings, and the dissolved pores were filled with calcite (Figure 3f). The second stage of dissolution only involved the dissolution of early ferrocalcite, and the dissolved pores were filled with late calcite (Figure 3c). The third stage of dissolution formed numerous pores that were visible. The dissolved minerals in this stage included illite (Figure 3f), chlorite (Figure 3o), plagioclase (Figure 3l), etc., among which the dissolution of illite and chlorite was usually accompanied by microcrystalline quartz, whereas the dissolution of feldspar was accompanied by kaolinite (Figure 3l).

4.2. Geochemical Data of Authigenic Minerals

4.2.1. Major Elements

The EPMA was performed on the particle coating, feldspar particles, calcite, and dolomite. The results are shown in Table 1. Late dolomite had a higher FeO content than early dolomite, and the relative content distribution was 17.82–25.45%. The content of late calcite was tested by the EPMA. However, the elemental composition of C1 was not identified. The element distribution of particle coating was determined, and even within the same coating, such as the numbers 1#3 and 1#4 in Table 1, the element distribution showed significant differences (Figure 4).

Table 1. The chemical composition (mass fraction, wt%) of minerals in the study area.

Well	Number *	Depth (m)	Mineral Characteristic	Na_2O	K_2O	MnO	MgO	SiO_2	FeO	CaO	SrO	CoO	SO_3	TiO_2	Al_2O_3	Cr_2O_3	NiO	Total
Q9-3	1#1	2419	Ferrodolomite	1.19	0.00	0.30	24.00	0.09	21.44	52.93	0.00	0.02	0.03	/	/	/	/	100
Q9-3	1#2	2419	Ferrodolomite	0.96	0.02	0.75	20.67	0.09	25.17	51.94	0.24	0.09	0.07	/	/	/	/	100
Q9-3	1#3	2423	Ferrodolomite	0.39	0.01	0.63	22.73	0.35	20.35	55.41	0.13	0.00	0.00	/	/	/	/	100
Q9-3	1#4	2423	Ferrodolomite	0.32	0.02	0.70	22.61	0.17	17.82	58.07	0.21	0.08	0.01	/	/	/	/	100
Q9-3	2#7	2423	Ferrodolomite	1.07	0.00	0.72	23.81	0.06	21.71	52.45	0.12	0.06	0.00	/	/	/	/	100
Q9-3	2#8	2423	Ferrodolomite	0.29	0.00	0.90	20.96	0.05	23.41	54.10	0.25	0.00	0.03	/	/	/	/	100
Q9-3	2#1	2423	Early dolomite	0.06	0.04	0.00	40.07	0.04	0.11	59.69	0.00	0.00	0.01	/	/	/	/	100
Q9-3	2#2	2423	Early dolomite	0.09	0.00	0.04	39.26	0.11	0.13	60.38	0.00	0.00	0.00	/	/	/	/	100
Q9-3	1#1	2174	Calcite filled in pores	0.06	0.02	7.81	0.04	0.09	0.23	91.62	/	/	/	0.06	0.04	0.00	0.03	100
Q9-3	1#2	2174	Calcite filled in pores	0.04	0.03	8.44	0.07	0.08	0.10	91.22	/	/	/	0.00	0.01	0.00	0.00	100
Q9-3	1#3	2174	Particle coating	0.56	1.22	0.22	0.64	85.08	3.95	4.85	/	/	/	0.08	3.41	0.00	0.00	100
Q9-3	1#4	2174	Particle coating	1.28	7.39	0.10	3.28	59.57	11.28	1.84	/	/	/	0.46	14.78	0.02	0.00	100
Q9-3	2#2	2174	Particle coating	0.47	1.86	0.08	1.74	85.22	3.11	1.11	/	/	/	0.11	6.27	0.04	0.00	100
Q9-3	2#3	2174	Particle coating	0.87	5.06	0.00	2.60	71.27	6.35	0.54	/	/	/	0.17	13.10	0.04	0.00	100
Q9-3	2#5	2174	Calcite filled in pores	0.11	0.03	7.89	0.10	0.19	0.20	91.42	/	/	/	0.00	0.02	0.05	0.00	100
Q9-3	1#1	2424	Albite	11.26	0.07	0.01	0.00	67.83	0.11	0.33	/	/	/	0.00	20.38	0.01	0.00	100
Q9-3	1#5	2424	Potassium feldspar	0.87	14.90	0.00	0.00	65.10	0.09	0.01	/	/	/	0.01	19.02	0.00	0.00	100
Q9-3	2#1	2424	Ferrodolomite	1.06	0.04	0.72	20.98	0.06	25.45	49.75	/	/	/	0.03	1.86	0.05	0.00	100
Q9-3	2#5	2424	Kaolinite	0.29	0.19	0.02	0.03	54.02	0.13	0.11	/	/	/	0.00	45.17	0.03	0.01	100
Q9-3	2#7	2424	Kaolinite	0.24	0.19	0.00	0.03	53.37	0.08	0.04	/	/	/	0.00	46.00	0.02	0.04	100
Q9-3	3#1	2424	Overgrown quartz	0.03	0.00	0.00	0.00	99.74	0.08	0.01	/	/	/	0.00	0.10	0.04	0.00	100
Q9-3	3#2	2424	Ferrodolomite	1.02	0.01	0.90	21.86	0.31	21.80	52.33	/	/	/	0.00	1.65	0.05	0.07	100
Q9-3	3#4	2424	Early dolomite	0.01	0.03	0.06	42.83	0.10	0.10	56.84	/	/	/	0.00	0.01	0.00	0.03	100

* The meaning of the numbers: for example, in 1#2, 1 represents the sample number, and 2 represents the location number of the EPMA test conducted on sample 1.

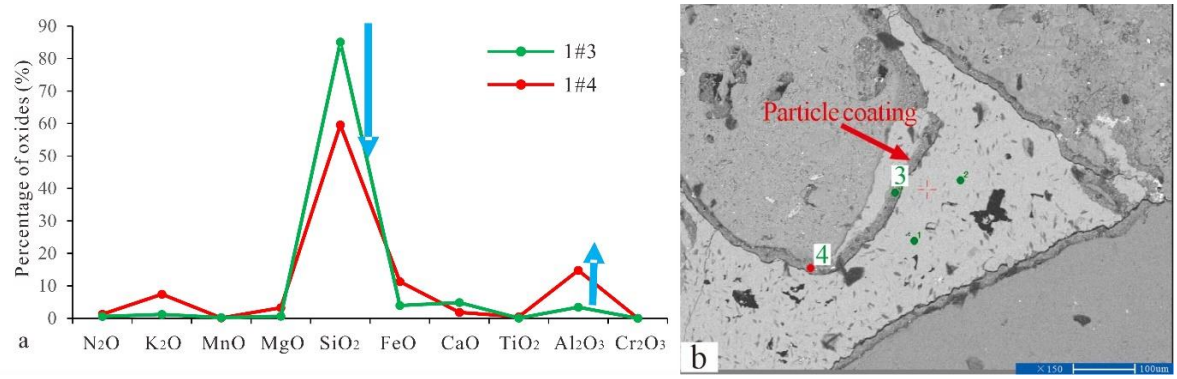


Figure 4. (**a**) The element composition of the coating in the sample of well Q9-3 (number: 1#3 and 1#4; the blue arrow indicates the element that has changed). (**b**) Test positions of 1#3 and 1#4 on the backscatter image.

4.2.2. Carbon and Oxygen Isotopes

The minerals tested by isotopes included calcite and dolomite. The isotopic data of various minerals are shown in Table 2. The distribution of carbon and oxygen isotopes differed considerably between C1 and C2, D1 and D2. The carbon and oxygen isotope distribution of C2 showed a negative shift compared to that of C1, and that of D2 showed a negative shift compared to the distribution of the isotopes in D1. The carbon and oxygen isotope distribution of calcite or dolomite was highly correlated (Figure 5).

Table 2. The micro isotopic data of carbonate minerals in the study area.

Well	Depth (m)	Mineral Type	$\delta^{13}C_{PDB}$ (‰)	$\delta^{18}O_{PDB}$ (‰)	Type
Q9-1D	2434.45	Dolomite	3.72	−7.56	D1
Q9-1D	2182.1	Dolomite	−3.08	−10.26	D2
Q9-1D	2183.67	Dolomite	−3.3	−10.66	D2
Q9-1D	2845.75	Dolomite	−2.56	−10.22	D2
Q9-1D	2848.56	Dolomite	−2.56	−11.26	D2
Q9-1D	2850.32	Calcite	1.13	−8.41	C1
Q9-2	1860.2	Calcite	5.02	−7.79	C1
Q9-2	2317.3	Calcite	4.23	−8.11	C1
Q9-3	2174.2	Calcite	3.52	−7.97	C1
Q9-3	2187.21	Calcite	−8.51	−13.32	C2
Q9-3	2211.9	Calcite	−12.59	−13.64	C2
Q9-3	2218.44	Calcite	−13.82	−13.89	C2
Q9-3	2214.94	Calcite	−15.44	−13.72	C2

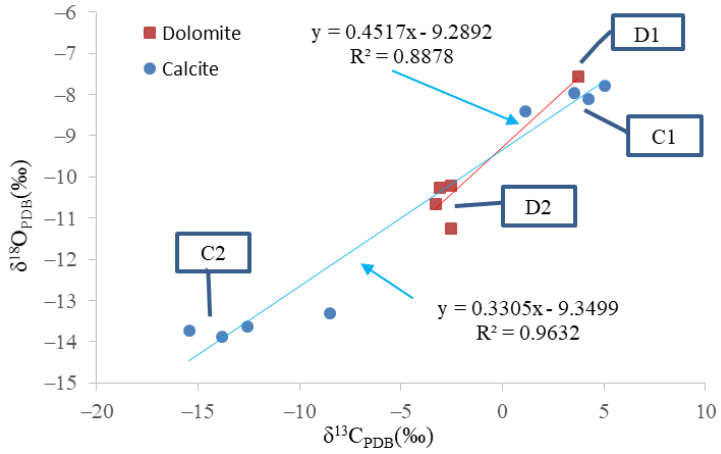


Figure 5. The distribution of the isotope of carbonate minerals; D1, D2, C1, and C2 represent early dolomite, ferrodolomite, ferrocalcite, and late calcite, respectively.

4.2.3. Homogenization Temperature of Inclusions

The homogenization temperature of inclusions can be used to indirectly record the formation time of authigenic minerals. In this study, we tested the homogenization temperature of the inclusions captured in authigenic quartz. The inclusions were captured in healed quartz cracks and overgrown quartz. The main frequency distributions corresponding to the homogenization temperatures of the inclusions at the two capture locations were 75–90 °C and 116–136° C. These temperature ranges were associated with the two stages of the development of silicosis (Figure 6).

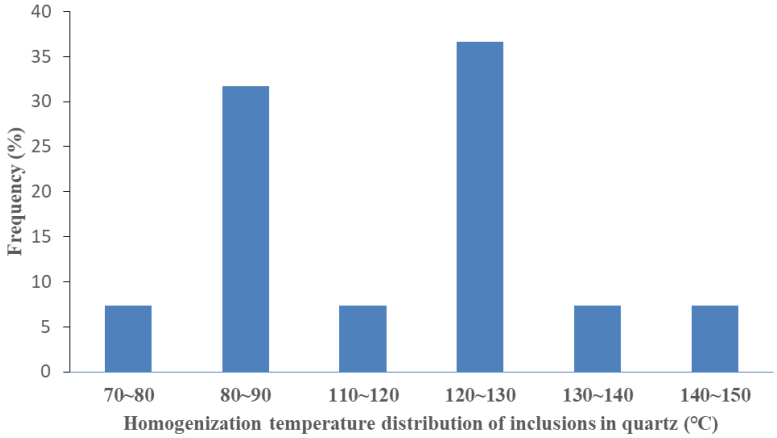


Figure 6. The homogenization temperature distribution of fluid inclusions.

5. Discussion

5.1. Indication of Isotopes to the Diagenetic Environment

Isotopes are the indicators of the fluid properties of sedimentation and diagenesis, and they are mainly affected by the temperature and salinity of the diagenetic environment [47].

5.1.1. The Salinity of Diagenetic Fluids

The Z distributions of the diagenetic fluids of D1 and C1 were 131.15 and 125.43–133.70, respectively, reflecting that the diagenetic fluids had high salinity. The Z distributions of D2 and C2 were 115.23–116.97 and 88.85–103.24, respectively, indicating that these diagenetic fluids had low salinity. The Z distribution was influenced by atmospheric freshwater or formation fluids [48].

5.1.2. The Temperature of Isotope Geology

The high correlation between the carbon and oxygen isotopes of carbonates in the study area indicated that the isotopic fractionation coefficients between minerals and fluids could be used for the inversion of the diagenetic temperature [48]. For temperature inversion, the $\delta^{18}O$ of the diagenetic fluid needs to be determined first. The Z-value characteristics showed that D1 and C1 were characterized by high salinity; D2 and C2 were characterized by low salinity. In this study, the oxygen isotope data of atmospheric fresh water ($\delta^{18}O_{SMOW}$ = −5‰), present seawater ($\delta^{18}O_{SMOW}$ = 0‰), and Jurassic seawater ($\delta^{18}O_{SMOW}$ range is −1.50‰–0.20‰) were used as references [18,49]. The $\delta^{18}O_{SMOW}$ values of the diagenetic fluids of D1 and C1 were about −2‰, and those of D2 and C2 were about −2.5‰. The isotopic geological temperatures of carbonate minerals calculated using equations 2 and 3 are shown in Figure 7. The temperature characteristics showed that the burial depths of D1 and C1 cementation were relatively shallow, and the temperature ranges were 62.3 °C and 45–48.7 °C, respectively. D2 and C2 cementation had deeper burial depths, and their respective temperature ranges were 78.2–86.7 °C and 79.3–83.9 °C.

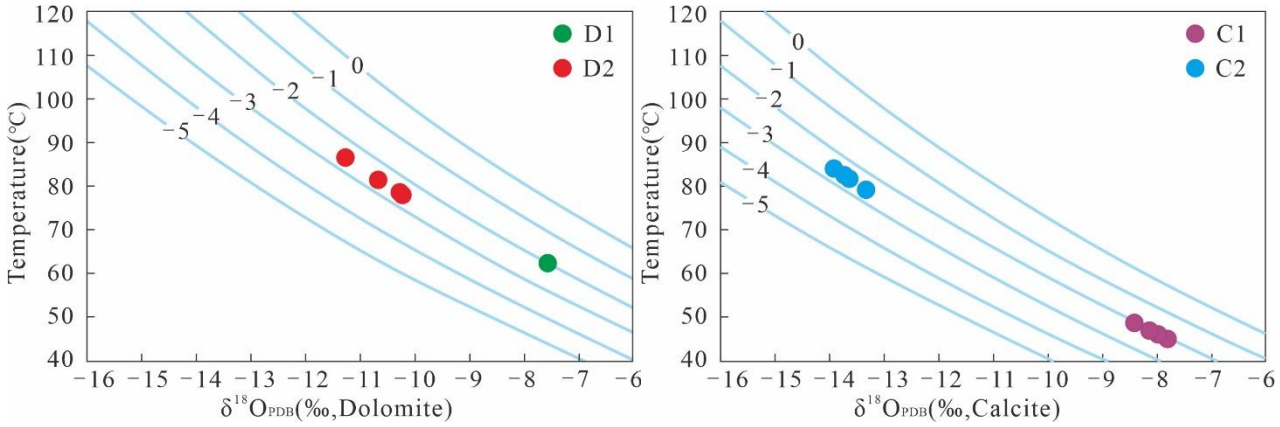


Figure 7. The geological temperature of the isotopes of calcite and dolomite; D1, D2, C1, and C2 represent early dolomite, ferrodolomite, ferrocalcite, and late calcite, respectively.

5.2. The Mechanism of Evolution of Diagenesis

5.2.1. The Mechanism of Evolution of Microcrystalline Quartz and Associated Clay Minerals

The particle coating remaining from the early dissolution was encapsulated by authigenic calcite (Figure 8a), which blocked the exchange of materials between the coating and the diagenetic fluid. Therefore, the encapsulated coating could indicate the composition of early interparticle matrices. The elemental characterization of the particle coating indicated that it was composed of silica-rich and illite-rich minerals (Figure 8b). The results of backscatter imaging showed that the silica-rich particle coating was amorphous silicon (Figure 4b) that was rich in K and poor in Na, which was different from the K_2O/Na_2O ratio of other authigenic minerals (Figure 9). The dispersed volcanic ash in the upper section of the Haifanggou Formation had a high content of unstable minerals. During deposition, dispersed volcanic ash might be chemically altered into smectite and silica, leading to the release of large quantities of K, Fe, Mg, and Ga and turning the solution alkaline [50,51]. In a K ion-rich alkaline environment, smectite is prone to alterations; it can absorb K ions and release SiO_2, forming illite $\left(Smectite + Al^{3+} + K^{+} \rightarrow Illite + SiO_2 + Ca^{2+} + Mg^{2+} + Na^{+} + Fe^{3+}\right)$. In the parts where the intergranular matrix was still preserved after dissolution, smectite continued forming illite and filled the pore with illite (Figure 3h). The Si ions released promoted the nucleation of amorphous silicon [16] and the formation of microcrystalline quartz (Figure 3h,i). The grain size of the microcrystalline quartz formed at this stage was generally below 2 μm. Diagenetic fluids rich in Si ions healed fissures in quartz. The homogeneous temperature of inclusions in the healed fractures of early quartz was 75–90 °C.

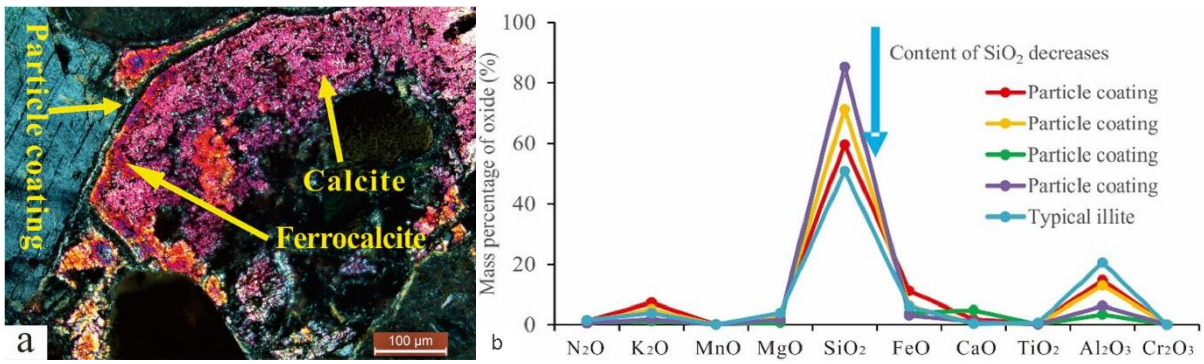


Figure 8. (**a**) The particle coating is coated with two-stage calcite, Q9-3, 2174.8 m. (**b**) Element distribution characteristics of particle coating and typical illite.

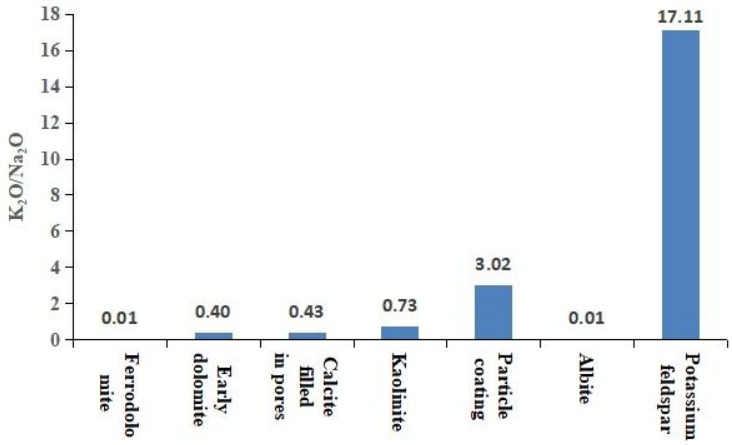


Figure 9. The distribution of the K_2O/Na_2O ratio of authigenic minerals.

The mineral combination of microcrystalline quartz and chlorite was grown together (Figure 3k). The shrinkage pores of tuffaceous mudstone strata in the Middle-Lower Jurassic were filled with chlorite (Figure 10), indicating that the strata during this burial period were in an alkaline (pH range: 7–9) reducing environment rich in iron and magnesium [52]. The burial depth at 80–95 °C corresponding to the Jurassic in the study area indicated the peak period of the generation and discharge of organic matter [41]. The buffering of the pH by easily soluble components, such as volcanic ash and mud, inhibited the increase in the H ion concentration in the diagenetic environment [2], and the discharged hydrocarbon fluids carried abundant Fe, Mg, and Ga to the sandstone reservoir. This process provided a suitable diagenetic environment for the transformation of illite into chlorite $\left(Illite + Mg^{2+} + Fe^{2+} \rightarrow Chlorite + K^{+} + H^{+} + SiO_2 + H_2O\right)$. The replacement of illite by chlorite confirms this type of diagenetic transformation (Figure 3k). The Si ions released during the conversion process promoted the continuous growth of microcrystalline quartz, resulting in the formation of microcrystalline quartz with a particle size of 2–5 μm. The change in the particle size occurred because chlorite was larger than microcrystalline quartz associated with illite (Figure 3j).

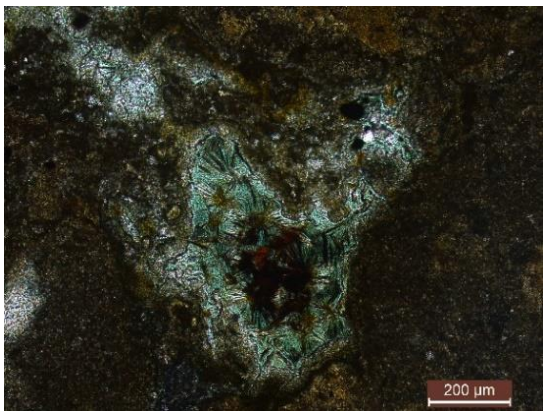


Figure 10. Chlorite filled in the shrinkage hole of tuff, Q9-3, 2175.43 m.

5.2.2. Mechanism of Dissolution

Although several studies have shown that the dissolution of atmospheric water in the supergene stage and the dissolution of organic acid caused by organic thermal evolution are necessary for the formation of high-quality reservoirs [41], the information on the timing and stage of dissolution is not known. Based on the understanding of the diagenetic mechanism, we provided a detailed description of dissolution.

The dissolution characteristics showed that the first stage of the dissolution pore was filled with C1, and the early calcite filling occurred after the dissolution of D1 (Figure 3c). The formation temperature distributions of D1 and C1 were 62.3 °C and 45.0–48.7 °C, respectively. The dissolution of this phase was the product of supergene weathering, which occurred because of the shallow burial depth at the time of dissolution, the decrease in temperature, and the tectonic uplift of the formation.

When the burial temperature in the study area was about 80 °C, organic matter released organic acids via thermal evolution [41]. Theoretically, organic acids can shift the pH of water between 5 and 6 [53]. However, the formation of chlorite (which occurs in an alkaline environment between pH 7 and 9) indicated that an acidic environment was not formed in this period. Thus, the buffer of soluble components, such as volcanic ash, inhibited the increase in the H ion concentration, and the local dissolution of a small amount of C1 in the study area confirmed that the dissolution intensity in this period was weak.

In the middle-deep burial stage of the study area, when the diagenetic temperature exceeded 100 °C, the decarboxylation of organic acids (mainly acetic acid) released a large quantity of CO_2 and organic acids ($RCOOHNO \rightarrow RH + CO_2$), which decreased the pH of pore water between 4 and 5 [2]. The acidic fluid formed could dissolve minerals such as feldspar and volcanic ash. The homogenization temperature of inclusions in overgrown quartz formed by feldspar dissolution (details in Section 5.2.5) was between 116 and 145 °C, indicating that the third stage of dissolution occurred later, and the temperature at which the dissolution started might be around 116 °C.

5.2.3. The Mechanism of Formation of Dolomite

1. Early Dolomite (D1)

We found that D1 was formed in a shallow burial diagenetic environment. The presence of micrite and powdered crystal of D1, occasionally with dolomitized oolites, and an isotopic geological temperature of 62.3 °C indicated that the environment was diagenetic. The results of the elemental analysis showed that D1 exhibited a distribution pattern that was comparable to particle coating (Figure 11), indicating that the material source was the same. Alterations in volcanic ash can provide abundant Ga and Mg ions and make the diagenetic environment alkaline. We found that the diagenetic material of D1 originated from the alteration of volcanic ash in the early stage of diagenesis.

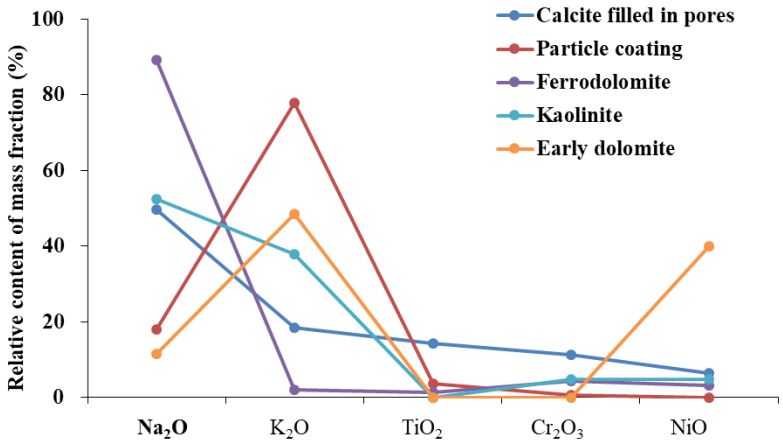


Figure 11. The partition patterns of some oxides of early dolomite and other minerals.

2. Late Ferrodolomite (D2)

The carbon and oxygen isotope composition of D2 was negative compared to that of D1. The negative shift of isotopes might be affected by the dilution of atmospheric freshwater and the strong water-rock interaction against the background of the increase in

burial temperature [54,55]. The microscopic features showed that D2 had coarse particles and an excellent rhombohedral crystal formation. This feature mainly occurred in the late diagenetic stage. As the isotopic geological temperature of D2 ranged from 78.2 °C to 86.7 °C, it was probably generated during the early stages of diagenetic stage B. During this period, smectite was converted into illite, which absorbed K ions and released Na, Ga, Fe, and Mg ions. The analysis of the major elements showed that the average values of MnO/FeO and K_2O/Na_2O of D2 were 0.03 and 0.13, respectively, which indicated that it was rich in Fe and Na ions. Thus, during early diagenetic stage B, the continuous conversion of smectite into illite provided abundant material for the cementation of D2.

5.2.4. The Mechanism of Formation of Calcite

1. Ferrocalcite (C1)

The oxygen isotope geological temperature of C1 was 45–48.7 °C, indicating that it formed in a shallow burial diagenetic environment. According to the $\delta^{13}C_{PDB}$-$\delta^{18}O_{PDB}$ distribution map of calcite in a continental sedimentary background (modified by Qing [56]), the carbon source of C1 was related to paleontological activities (Figure 12). The paleosalinity index (Z) of C1 (ranging from 125.43 to 133.70) showed that the diagenetic fluid had high salinity, which might be related to the relatively open diagenetic environment. The diagenetic sequence showed that the cementation of C1 occurred after the epigenetic karst. Following the epidiagenetic stage, Qikou Sag received deposition from the third section of the Shahejie Formation [57]. The Shahejie Formation in the Bohai Bay Basin had several transgression events [58]. This indicated that there were many saltwater sedimentary environments in the study area after the epidiagenetic stage. Based on the above-mentioned findings, we inferred that high salinity fluid has a high biological yield under the influence of transgression in the relatively open shallow burial environment, and the activities of archaea such as halophilic bacteria and sulfate-reducing bacteria can become an important factor in the carbon cycle. For example, inorganic C and Ga ions can be produced by bacterial sulfate reduction, which typically occurs in a shallow burial diagenetic environment at 0–60 °C [59,60]. The cementation of C1 occurred in an ion-rich, suitable diagenetic environment.

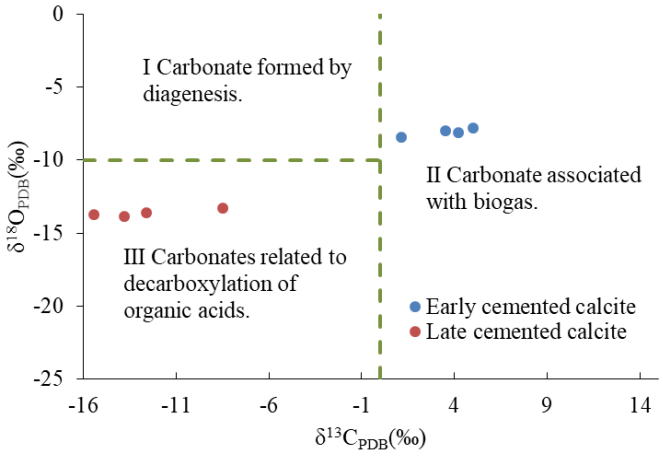


Figure 12. A scatter plot of $\delta^{13}C_{PDB}$ and $\delta^{18}O_{PDB}$ of calcite.

2. Late Dolomite (C2)

The isotopic geological temperature of C2 was 79.3–83.9 °C, which corresponded to the period of generation and discharge of large quantities of organic matter. Generally, the $\delta^{13}C_{PDB}$ of CO_2 was formed by the thermal cracking of kerogen when the temperature exceeded 70 °C and was between −10% and −20%. The mixing of carbon isotopes of organic origin and sedimentary sources generally caused a negative offset of the carbon isotope value of the diagenetic fluid. The $\delta^{13}C_{PDB}$-$\delta^{18}O_{PDB}$ distribution map of calcite showed that the carbon sources of C2 were related to the decarboxylation of organic acids (Figure 12). The characteristics of the element showed that the average MnO/FeO value of C2 was 47.78, which was rich in Mn and poor in Fe. As mentioned earlier, the conversion of illite into chlorite required a large amount of Fe and Mg, which substantially decreased the quantity of Fe ions present. Our findings showed that the ion-rich fluid discharged by the release of formation pressure provided favorable conditions for the cementation of D2.

5.2.5. Formation Mechanism of Overgrown Quartz

The sources of Si are primarily used to identify the origins of overgrown quartz. Sources of silicon (Si) include dissolved biological silicon, quartz that has been dissolved and then re-crystallized, altered clay minerals, dissolved feldspar, and altered volcanic ash [61–63]. The microscopic characteristics showed that silicon-rich organisms and stylolite formed by pressure dissolution were absent, while the upper section was rich in clay minerals and minerals in altered volcanic ash. The characteristics of the element showed that the origin of the silicon in volcanic ash was quite different from that of overgrown quartz (Figure 13). In the development area of overgrown quartz, diagenesis showed the combined characteristics of "large amounts of plagioclase dissolution, developed authigenic kaolinite, and overgrown quartz". The reaction of plagioclase dissolution can be expressed by the formula $2NaAlSi_3O_8 + 2H^+ + H_2O \rightarrow Al_2Si_2O_5(OH)_4 + 2Na^+ + 4SiO_2$, and can release abundant Na ions while forming kaolinite and quartz. The distribution pattern of the element content of overgrown quartz and kaolinite was similar (Figure 14). The characteristics of the elements showed that the two minerals had the same origin. To summarize, the building blocks of overgrown quartz originated from the dissolution of plagioclase. The homogenization temperature of the inclusions showed that the peak temperature of this type of diagenesis is 116–136 °C.

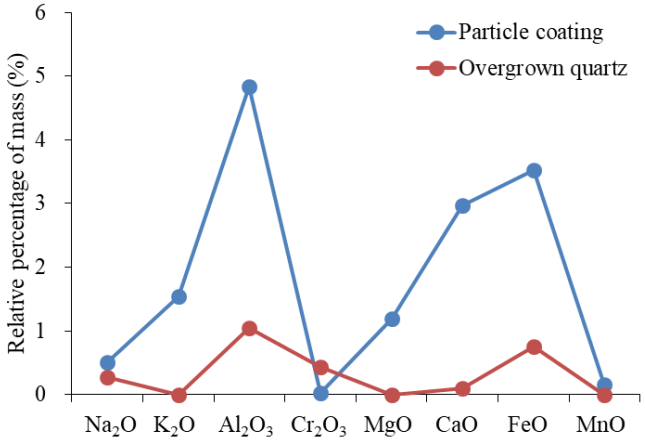


Figure 13. Composition distribution of particle coating and overgrown quartz.

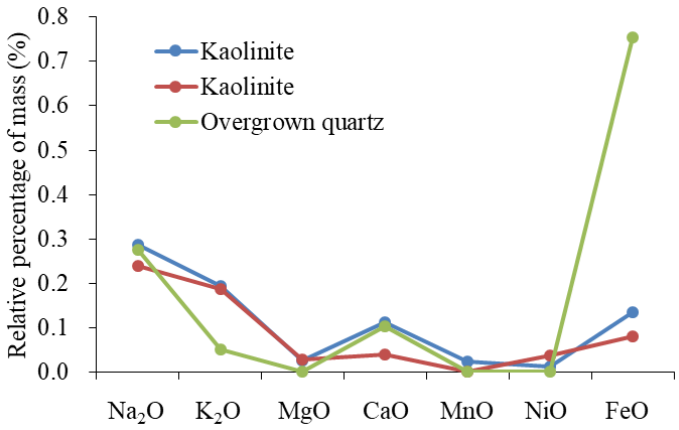


Figure 14. Compositional distribution patterns of overgrown quartz and kaolinite.

5.3. Sequence of Diagenetic Evolution

The diagenetic evolutionary sequence of the study area was established based on the relative occurrence of authigenic minerals (Figure 15). According to the geological characteristics of the study area, the diagenetic evolution of tuffaceous sandstone reservoirs that have undergone epigenetic karst can be divided into the following processes.

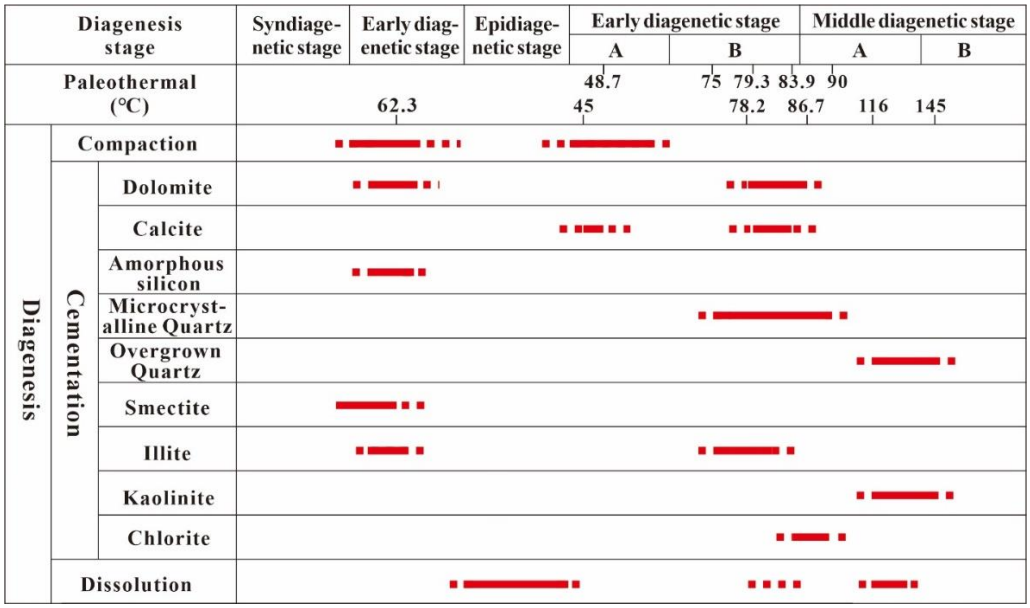


Figure 15. The sequence of the diagenetic evolution of reservoirs.

1. The Middle-Lower Jurassic Haifanggou Formation was rich in volcanic ash. The dissolution and alteration of volcanic materials formed a highly saline and alkaline environment [50].
2. The alkaline environment during deposition promoted the conversion of volcanic ash to smectite or illite/smectite mixed minerals while releasing an abundance of ions. During mineral transformation, silica-rich and illite-rich minerals were differentiated, forming illite/smectite mixed minerals and amorphous silicon.
3. In the shallow burial stage (the formation temperature was about 62.3 °C), the high salinity diagenetic fluid and suitable diagenetic environment promoted the cementation of early dolomite.

4. The late Cretaceous was affected by the Yanshan tectonic movement. The strata investigated in this study suffered about 20 Ma of exposure weathering [38,64]. The leaching of atmospheric water caused the first stage of karstification.
5. During the initial burial stage after the epidiagenetic stage, i.e., the sedimentary stage of the Shahejie Formation, several transgression events occurred, and highly saline fluid had a high biological yield under the influence of transgression. Paleontological activities generated large quantities of carbon and calcium ions. When the formation temperature reached 45.0–48.7 °C (early diagenetic stage A), the cementation of early calcite was formed.
6. With the increase in the burial depth, large quantities of smectite were transformed into illite. In the process of diagenetic transformation, the enrichment of Si released promoted the transformation of amorphous silicon to microcrystalline quartz, and the released Ca, Mg, and Fe formed late dolomite at about 75 °C.
7. When the burial temperature reached 80 °C, early diagenetic stage B transitioned to middle diagenetic stage A. The fluid released during the thermal evolution of organic materials was buffered by soluble components, which prevented the formation of a large acidic environment. However, the ions carried by the fluid promoted the transformation of illite to chlorite and the formation of late calcite.
8. When the diagenetic temperature exceeded 100 °C, the thermocatalytic stage was reached. The thermal catalytic decarboxylation of organic matter led to the release of organic acids and CO_2, which resulted in the dissolution of minerals by organic acids. The dissolved material caused the cementation of kaolinite and overgrown quartz at 116–145 °C, which was associated with the late stage of middle diagenetic stage A and the start of the transition to middle diagenetic stage B.

6. Conclusions

The Haifanggou Formation in Qikou Sag underwent compaction, cementation, and the transformation and dissolution of clay minerals during the burial process. Carbonate cementation included early ferrocalcite (C1), dolomite (D1), late calcite (C2), and ferrodolomite (D2). The cementation of quartz included the precipitation of microcrystalline quartz and the overgrowth of quartz. Clay minerals included smectite, illite, chlorite, and kaolinite. Dissolution occurred in three stages.

Supergene weathering was the first stage of dissolution. When the formation temperature reached 80 °C, the second stage of dissolution occurred facilitated by the acidic fluid released during the hydrocarbon generation process from organic matter. However, the acidic fluid was neutralized by soluble substances in the volcanic ash; thus, the second stage of dissolution was weak. When the diagenetic temperature exceeded 100 °C, the organic acidic fluid generated by the thermal cracking of organic matter and the acidic fluid rich in CO_2 contributed to the third stage of dissolution.

In the diagenetic period before the epidiagenetic stage, the alteration of volcanic ash promoted the formation of an alkaline environment and the transformation of volcanic ash to smectite or illite/smectite mixed minerals. The ions released by the alteration of volcanic ash led to the cementation of amorphous silica and early dolomite. In the initial burial stage after the epidiagenetic stage, transgression promoted a high biological yield, which provided a suitable diagenetic environment for early calcite cementation. With the deepening of burial, smectite continuously transformed into illite, and the ions released in this process promoted the formation of microcrystalline quartz and the cementation of late dolomite. The burial temperature of the stratum was about 80 °C, and the ions carried by the fluid released during the hydrocarbon generation process promoted the transformation of illite into chlorite and the formation of late calcite. The material source of the overgrown quartz was feldspathic dissolution, which occurred in the third stage of dissolution. This stage also provided the raw materials for the formation of kaolinite.

Author Contributions: Conceptualization, Z.L.; methodology, Z.L. and X.S.; software, C.Z. and J.R.; validation, Z.L. and C.Z.; formal analysis, P.H., Y.H. and W.Z.; investigation, X.S.; resources, Z.L.; data curation, Z.L.; writing—original draft preparation, X.S.; writing—review and editing, Z.L. and X.S.; visualization, Y.Q.; project administration, Z.L.; funding acquisition, Z.L. All authors have read and agreed to the published version of the manuscript.

Funding: This research was funded by National Science and Technology Major Project (grant number: 2016ZX05024-003).

Data Availability Statement: Not applicable.

Conflicts of Interest: The authors declare no conflict of interest.

References

1. Gao, Z.; Feng, J.; Cui, J.; Wang, X.; Zhou, C.; Shi, Y. Physical simulation and quantitative calculation of increased feldspar dissolution pores in deep reservoirs. *Pet. Explor. Dev.* **2017**, *44*, 359–369. [CrossRef]
2. Yuan, G.; Cao, Y.; Gluyas, J.; Cao, X.; Zhang, W. Petrography, fluid-inclusion, isotope, and trace-element constraints on the origin of quartz cementation and feldspar dissolution and the associated fluid evolution in arkosic sandstones. *AAPG Bull.* **2018**, *102*, 761–792. [CrossRef]
3. Yuan, G.; Cao, Y.; Qiu, L.; Chen, Z. Genetic mechanism of highquality reservoirs in Permian tight fan delta conglomerates at the northwestern margin of the Junggar Basin, northwestern China. *AAPG Bull.* **2017**, *101*, 1995–2019. [CrossRef]
4. Lima, R.D.; De Ros, L.F. The role of depositional setting and diagenesis on the reservoir quality of Devonian sandstones from the Solimões Basin, Brazilian Amazonia. *Mar. Pet. Geol.* **2002**, *19*, 1047–1071. [CrossRef]
5. Zhu, G.Y.; Zhang, S.C.; Chen, L.; Yang, H.J.; Yang, W.J.; Zhang, B.; Su, J. Coupling relationship between natural gas charging and deep sandstone reservoir formation: A case from the Kuqa Depression, Tarim Basin. *Pet. Explor. Dev.* **2009**, *36*, 347–357.
6. Bloch, S.; Lander, R.H.; Bonnell, L. Anomalously high porosity and permeability in deeply buried sandstone reservoirs: Origin and predictability. *AAPG Bull.* **2002**, *86*, 301–328.
7. Li, H.; Tang, H.M.; Qin, Q.R.; Zhou, J.L.; Qin, Z.J.; Fan, C.H.; Su, P.D.; Wang, Q.; Zhong, C. Characteristics, formation periods and genetic mechanisms of tectonic fractures in the tight gas sandstones reservoir: A case study of Xujiahe Formation in YB area, Sichuan Basin, China. *J. Pet. Sci. Eng.* **2019**, *78*, 723–735. [CrossRef]
8. Susanne, G.; Richard, H.W.; William, D.J.; Hans, K. Diagenesis and reservoir quality of Miocene sandstones in the Vienna Basin, Austria. *Mar. Pet. Geol.* **2008**, *25*, 681–695.
9. Islam, M.A. Diagenesis and reservoir quality of Bhuban sandstones (Neogene), Titas Gas Field, Bengal Basin, Bangladesh. *J. Asian Earth Sci.* **2009**, *35*, 89–100. [CrossRef]
10. Ajdukiewicz, J.M.; Nicholson, P.H.; Esch, W.L. Prediction of deep reservoir quality using early diagenetic process models in the Jurassic Norphlet Formation, Gulf of Mexico. *AAPG Bull.* **2010**, *94*, 1189–1227. [CrossRef]
11. Mansurbeg, H.; Morad, S.; Salem, A.; Marfil, R.; El-ghali, M.A.K.; Nystuen, J.P.; Caja, M.A.; Amorosi, A.; Garcia, D.; La Iglesia, A. Diagenesis and reservoir quality evolution of palaeocene deep-water, marine sandstones, the Shetland-Faroes Basin, British continental shelf(Article). *Mar. Pet. Geol.* **2008**, *25*, 514–543. [CrossRef]
12. Li, H.; Zhou, J.L.; Mou, X.Y.; Guo, H.X.; Wang, X.X.; An, H.Y.; Mo, Q.W.; Long, H.Y.; Dang, C.X.; Wu, J.F.; et al. Pore structure and fractal characteristics of the marine shale of the Longmaxi Formation in the Changning Area, Southern Sichuan Basin, China. *Front. Earth Sci.* **2022**, *10*, 1018274. [CrossRef]
13. Li, H. Research progress on evaluation methods and factors influencing shale brittleness: A review. *Energy Rep.* **2022**, *8*, 4344–4358. [CrossRef]
14. Taylor, T.R.; Giles, M.R.; Hathon, L.A. Sandstone diagenesis and reservoir quality prediction: Models, Myths, and reality. *AAPG Bull.* **2020**, *94*, 1093–1132. [CrossRef]
15. Areeq, N.M.A.; Soliman, M.A.; Essa, M.A.; Al-Azazi, N.A. Diagenesis and reservoir quality analysis in the Lower Cretaceous Qishn sandstones from Masila oilfields in the Sayun–Masila Basin, eastern Yemen. *Geol. J.* **2016**, *51*, 405–420. [CrossRef]
16. French, M.W.; Worden, R.H.; Mariani, E.; Larese, R.E.; Mueller, R.R.; Kliewer, C.E. Microcrystalline Quartz Generation and the Preservation of Porosity In Sandstones: Evidence from the Upper Cretaceous of the Subhercynian Basin, Germany. *J. Sediment. Res.* **2012**, *82*, 422–434. [CrossRef]
17. Worden, R.H.; French, M.W.; Mariani, E. Amorphous silica nanofilms result in growth of misoriented microcrystalline quartz cement maintaining porosity in deeply buried sandstones. *Geology* **2012**, *40*, 179–182. [CrossRef]
18. Lv, Z.; Yang, X.; Qing, Y.; Ye, S. Water-rock-hydrocarbon interactions in the Middle Jurassic Shaximiao Formation sandstones, Western Sichuan. *Oil Gas Geol.* **2015**, *36*, 545–554.
19. Shen, Z.; Liu, S.; Lv, Z.; Luo, X.; Gong, Y. Vertical Geochemical Characteristics of Continental Formation Water and Its Water-Rock Interaction in the Middle Area of Western Sichuan Depression. *Acta Sedimentol. Sin.* **2011**, *29*, 495–502.
20. Huang, T.C. A volcanic sedimentation model: Implications of processes and responses of deep-sea ashes. *Mar. Geol.* **1980**, *38*, 103–122. [CrossRef]

21. Scudder, R.P.; Murray, R.W.; Kutterolf, S.; Schindlbeck, J.C.; Underwood, M.B.; Wang, K.L. Sedimentary inputs to the nankai subduction zone: The importance of dispersed ash. *Geosphere* **2018**, *14*, 1451–1467. [CrossRef]
22. White, R.J.; Spinelli, G.A.; Mozley, P.S.; Dunbar, N.W. Importance of volcanic glass alteration to sediment stabilization: Offshore Japan. *Sedimentology* **2011**, *58*, 1138–1154. [CrossRef]
23. Khalaf, E.E.D.A.H. Diagenetic evolution of the volcaniclastic deposits: An example from neoproterozoic dokhan volcanics in wadi queih basin, central eastern desert, Egypt. *Arab. J. Geosci.* **2014**, *7*, 2603–2624. [CrossRef]
24. Tari, G.; Vrsic, A.; Gumpenberger, T.; Mekonnen, E.; Enukidze, O. Eocene volcaniclastics in the kartli basin, georgia: A fractured reservoir sequence. *J. Pet. Geol.* **2021**, *44*, 413–433. [CrossRef]
25. Lenhardt, N.; Götz, A.E. Volcanic settings and their reservoir potential: An outcrop analog study on the Miocene Tepoztlán Formation, Central Mexico. *J. Volcanol. Geotherm. Res.* **2011**, *204*, 66–75. [CrossRef]
26. Wang, H.Y.; Fan, T.l.; Xiao, Y.Y.; Chen, J.; Nie, W.B. Effect of tuffaceous components on physical property of sandstone reservoir. *Acta Pet. Sin.* **2010**, *31*, 432–439.
27. Zeng, X.Y.; Zhang, J.; Liu, Y.Y.; Li, Y. Significance of syndepositional volcanism to high quality reservoirs in the Xujiahe Formation, the western Sichuan Depression. *Oil Gas Geol.* **2012**, *33*, 50–60.
28. Meng, Q.A.; Li, J.H.; Li, Y.; Zou, Y. Genetic mechanism os high content Tuffaceous clastic rock reservoir in Hailar-Tamucage Basin. *J. Jilin Univ.* **2020**, *50*, 569–578.
29. Moscariello, A.; Segvic, B.; Lehu, R.; Pedersen, G.; Gonus, J.; Arbiol, C.; Limeres, A.; Bernhardt, C.; Perez, D.; Thompson, A.; et al. New Insights on the Characterisation of the Pyroclastic-rich Bajo Barreal Fluvial Reservoir (Argentina). In Proceedings of the 78th EAGE Conference & Exhibition, Vienna, Austria, 30 May–2 June 2016.
30. Payana, K.D.; Karimullah, A.R.; Fahmita, R.; Titisari, A.D. Mineralogy Variation of Zeolites, Structural Deformation and its Impact to Tuffaceous Sandstone Diagenetic Anomaly in Kebo-Butak Formation, Sumberan, Yogyakarta. *Mater. Sci. Forum* **2017**, *901*, 197–203. [CrossRef]
31. Wang, E.; Liu, G.; Pang, X.; Li, C.; Wu, Z. Diagenetic evolution and formation mechanisms of middle to deep clastic reservoirs in the Nanpu sag, Bohai Bay Basin, East China. *Pet. Explor. Dev.* **2020**, *47*, 321–333. [CrossRef]
32. Li, J.; Wei, P.; Shi, L.; Chen, G.; Peng, W.; Sun, S.; Zhang, B.; Xie, M.; Hong, L. Fluid interaction mechanism and diagenetic reformation of basement reservoirs in Beier Sag, Hailar Basin, China. *Pet. Explor. Dev.* **2020**, *47*, 45–56. [CrossRef]
33. Anthony, J.P. Water-rock interaction and Reactive-transport modeling using elemental mass-balance approach: I. the methodology. *Am. J. Sci.* **2014**, *314*, 785–804.
34. Teng, C.Y.; Zou, H.Y.; Hao, F. Control of differential tectonic evolution on petroleum occurrence in Bohai Bay Basin. *Sci. China Earth Sci.* **2014**, *57*, 1117–1128. [CrossRef]
35. Yuan, G.; Cao, Y.; Gluyas, J.; Li, X.; Xi, K.; Wang, Y.; Jia, Z.; Sun, P.; Oxtoby, N.H. Feldspar dissolution, authigenic clays, and quartz cements in open and closed sandstone geochemical systems during diagenesis: Typical examples from two sags in Bohai Bay Basin, East China. *AAPG Bull.* **2015**, *99*, 2121–2154. [CrossRef]
36. Bo, S.; Zhang, J.; Hang, G.; Liang, C.; Guo, Z. Differential evolution of south and north structure in Huanghua Depression. *Bull. Sci. Technol.* **2022**, *38*, 20–25.
37. Xiao, S.; Lv, D.; Hou, M.; Hu, H.; Huang, Z. Mesozoic tectonic evolution and buried hill formation mechanism in the southwestern Bohai Sea. *Nat. Gas Ind.* **2019**, *39*, 34–44.
38. Wang, W.; Zheng, Y.; Feng, J.; Lou, D.; Wang, J.; Jia, L. Distribution of buried hill and exploration direction of hydrocarbon in Qikou Sag. *Mud Logging Eng.* **2012**, *23*, 93–97.
39. Ma, Y.; Sun, Y.; Ma, Y.; Jiang, W.; Sun, X. Tectonic evolution and genesis of fault zones in Qikou sag, Bohai Bay Basin. *Acta Pet. Sin.* **2020**, *41*, 526–539.
40. Guo, Y.; Wang, Y.; Peng, J.; Gao, K.; Wu, Q.; Wu, H. Main controlling factors on the formation of high-quality reservoirs in the Middle and Lower Jurassic clastic rock buried hills in Qinan fault terrace belt, Bohai sea. *China Offshore Oil Gas* **2018**, *30*, 41–50.
41. Zhao, Q.; Zhao, G.; Wan, L.; Fan, J.; Wang, X. The controlling factors of Jurassic high quality reservoirs in Qinan fault step belt of Bohai Sea. *Mar. Geol. Front.* **2015**, *31*, 28–35.
42. Lu, H.; Xu, C.; Wang, Q.; Du, X.; Liu, X. Genetic mechanism of carbonate cements and its impact on the Mesozoic clastic reservoir quality of the C12 and Q17 structures, Bohai Sea Area. *Oil Gas Geol.* **2019**, *40*, 1270–1280.
43. Li, Z.; Li, J.; Cui, J.; Xing, L.; Wu, X. The reservoir characteristics and main controlling factors of the Mesozoic clastic reservoirs in buried hill, Beidagang, Bohai Bay Basin. *Nat. Gas Geosci.* **2020**, *31*, 13–25.
44. Keith, M.L.; Weber, J.N. Carbon and oxygen isotopic composition of selected limestones and fossils. *Geochim. Cosmochim. Acta* **1964**, *28*, 1787–1816. [CrossRef]
45. Friedman, I.; O'Nei, J.R. *Compilation of Stable Isotope Fractionation Factors of Geochemical Interest*; Data of Geochemistry, 6th edn 1977; Geological Survey Professional Paper 440-KK.; US Government Printing Office: Washington, DC, USA, 1977.
46. Fisher, R.S.; Land, L.S. Diagenetic history of Eocene Wilcox sandstones, South-Central Texas. *Geochim. Cosmochim. Acta* **1986**, *50*, 551–561. [CrossRef]
47. Huang, S. *Carbonate of Diagenesis*; Geological Publishing House: Beijing, China, 2010; Volume 81–84, pp. 54–66.
48. Liu, S.; Shen, Z.; Liu, H.; Lv, Z.; Wang, P. Mechanism of water-rock interaction of the Upper Triassic Xujiahe Formation in the middle part of western Sichuan depression. *Acta Pet. Sin.* **2013**, *34*, 47–58.

49. Veizer, J.; Ala, D.; Azmy, K.; Bruckschen, P.; Buhl, D. 87Sr/86 Sr, d13C and d18O evolution of Phanerozoic seawater. *Chem. Geol.* **1999**, *161*, 59–88. [CrossRef]
50. Chipera, S.J.; Goff, F.; Goff, C.J.; Fittipaldo, M. Zeolitization of intracaldera sediments and rhyolitic rocks in the 1.25 Ma lake of Valles caldera, New Mexico, USA. *J. Volcanol. Geotherm. Res.* **2008**, *178*, 317–330. [CrossRef]
51. Yu, Z.; Cheng, R.; Zhau, X.; Sun, F. Types and Succession of Pyroclastic Rocks Diagenesis in Lower Cretaceous of Wuerxun and Bei'er Depression in Hailaer Basin. *Earth Sci. J. China Univ. Geosci.* **2012**, *37*, 851–859.
52. Tian, J.; Chen, Z.; Yang, Y. Protection Mechanism of Authigenic Chlorite on Sandstone Reservoir Pores. *Geol. Sci. Technol. Inf.* **2008**, *27*, 49–54.
53. Yuan, G.; Cao, Y.; Xi, K.; Wang, Y.; Li, X.; Yang, T. Feldspar dissolution and its impact on physical properties of Paleogene clastic reservoirs in the northern slope zone of the Dongying sag. *Acta Pet. Sin.* **2013**, *34*, 853–866.
54. Shah, M.M.; Ahmed, W.; Ahsan, N.; Lisa, M. Fault-controlled, bedding-parallel dolomite in the middle Jurassic Samana Suk Formation in Margalla Hill Ranges, Khanpur area (North Pakistan): Petrography, geochemistry, and petrophysical characteristics. *Arab. J. Geosci.* **2016**, *09*, 405. [CrossRef]
55. Zhang, B. *Geology and Genesis of Marine Carbonate Reservoirs in China*; Science Press: Beijing, China, 2017; Volume 1, pp. 471–475, ISBN 978-7-03-053045-5.
56. Qing, Y.H.; Lv, Z.X.; Wu, J.Y.; Yang, J.J.; Zhang, S.L.; Xiong, C.H.; Liu, J.F. Formation mechanisms of calcite cements in tight sandstones of the Jurassic Lianggaoshan Formation, northeastern Central Sichuan Basin. *Aust. J. Earth Sci.* **2019**, *66*, 723–740. [CrossRef]
57. Lang, J. Research on exploration and estimation technologies for subtle reservoir in slope of Qikou sag. Ph.D. Thesis, China University of Geosciences, Beijing, China, 2008.
58. Wei, W.; Algeo, T.J.; Lu, Y.C.; Liu, H.M.; Zhang, S.P.; Zhang, J.Y.; Du, Y.S. Paleosalinity Proxies and Marine Incursions into the Paleogene Bohai Bay Basin Lake System, Northeastern China. *Acta Sedimentol. Sin.* **2021**, *39*, 571–592.
59. Hu, H.; Li, H.; Xu, P.; Tao, L.; Hua, X. Main controlling factors of differential enrichment of oil and gas in fault concentrated zones:a case study from Qinan step-fault zone in Qikou Sag. *Lithol. Reserv.* **2020**, *32*, 34–45.
60. Zhang, F.; Zhang, S.; Qi, J.; Zhang, Y.; Song, S. Bacterial Mechanism of the Development of Sulfate Karst in Burial Environment. *Earth Sci.-J. China Univ. Geosci.* **2010**, *35*, 146–154.
61. Zhang, S.; Lv, Z.; Xiong, C.; Ji, P.; Qi, Y. Characteristics and Formation Mechanism of Jurassic Microcrystalline Quartz Coating in Qikou Sag. *Xinjiang Pet. Geol.* **2018**, *39*, 537–541.
62. Beard, D.C.; Weyl, P.K. Influence of Texture on Porosity and Permeability of Unconsolidated Sand. *AAPG Bull.* **1973**, *57*, 349–369.
63. Li, J.; Li, H.; Yang, C.; Wu, Y.J.; Gao, Z.; Jiang, S.L. Geological characteristics and controlling factors of deep shale gas enrichment of the Wufeng-Longmaxi Formation in the southern Sichuan Basin, China. *Lithosphere* **2022**, *2022*, 4737801. [CrossRef]
64. Peng, C.; Lin, H.; Liu, H.; Wu, Z.; Liu, G. Tectonic Evolution of the Bohai Bay Basin and the Palaeozoic Original Oil and Gas Reservoirs. *Geol. J. China Univ.* **2008**, *14*, 206.

Disclaimer/Publisher's Note: The statements, opinions and data contained in all publications are solely those of the individual author(s) and contributor(s) and not of MDPI and/or the editor(s). MDPI and/or the editor(s) disclaim responsibility for any injury to people or property resulting from any ideas, methods, instructions or products referred to in the content.